Appearance of a peak in the symmetry energy at $N = 126$ for the Pb isotopic chain within the relativistic energy density functional approach

Jeet Amrit Pattnaik,[1,*] Joshua T. Majekodunmi,[2,†] Ankit Kumar,[3,4,‡] M. Bhuyan,[5,§] and S. K. Patra[3,4,‖]

[1]*Department of Physics, Siksha "O" Anusandhan, Deemed to be University, Bhubaneswar 751030, India*

[2]*Institute of Engineering Mathematics, Faculty of Applied and Human Sciences, Universiti Malaysia Perlis, Arau 02600, Perlis, Malaysia*

[3]*Institute of Physics, Sachivalya Marg, Bhubaneswar 751005, India*

[4]*Homi Bhabha National Institute, Training School Complex, Anushakti Nagar, Mumbai 400094, India*

[5]*Center for Theoretical and Computational Physics, Department of Physics, Faculty of Science, University of Malaya, Kuala Lumpur 50603, Malaysia*

(Received 6 October 2021; revised 14 November 2021; accepted 11 January 2022; published 21 January 2022)

The newly derived relativistic energy density functional [Phys. Rev. C **103**, 024305 (2021)], which stems from the effective field theory motivated relativistic mean field (E-RMF), is employed to establish the appearance of peaks and/or kinks in the symmetry energy over the isotopic chain of Pb nuclei. The coherent density fluctuation model parametrization procedure for finite nuclei is adopted here to obtain the relativistic energy density functional at local density. The relativistic energy density functional from relativistic mean-field theory takes precedence over the Brückner energy density functional as it accurately predicts the empirical saturation density and binding energy per nucleon E/A, so-called coester band problem. Interestingly, using the relativistic energy density functional, it is possible to predict the peak at $N = 126$ for recently developed G3 and widely used NL3 parameter sets, which is not observed for Brückener's functional in spite of using the relativistic mean-field density. From the present analysis, the newly fitted energy density functional is found to be minutely sensitive to the choice of the parameter sets employed.

DOI: 10.1103/PhysRevC.105.014318

I. INTRODUCTION

The study of nuclear symmetry energy and its isospin dependence is of central interest in various areas of nuclear physics [1–4] and astrophysical systems including neutron stars [5,6]. This is one of the most essential characteristics of nuclei that are far from the stability line. Several recent studies have unequivocally demonstrated that the presence of kinks in the symmetry energy of finite nuclei over the isotopic chain points to the existence of magic numbers [7–12]. The advancement in the sophisticated experimental radioactive ion beam facilities using the projectile-fragmentation reaction method with fast ion-beams at FRIB (USA) [13], RIKEN (Japan) [14], GSI (Germany) [15], FLNR (Russia) [16], CSR (China) [17], and SPIRAL2/GANIL (France) [18] have led to a renaissance of investigating the behavior of symmetry energy at and above the saturation density [19]. An alternative way to produce the radioactive ion beam is the isotope separator online (ISOL) technique, which has recently gained momentum for highly asymmetric isospin nuclei [20]. The notable examples among them are at Lou-vain la Neuve (Belgium) [21], Spiral (France) [22], Alto (France) [23,24], ISAC (Canada) [25], and REX ISOLDE (Switzerland/France) [26]. In this context, the symmetry energy is closely associated with the isospin asymmetry of both finite and infinite nuclear matter, and hence serves as a bridge between them [27]. To predict this isospin and density-dependent quantity, the so-called symmetry energy for both infinite nuclear matter and finite nuclei, one has to use a reliable and convenient approach that works in a wide range of densities, i.e., from sub- to suprasaturation density.

Conventionally, various approaches such as the liquid drop model [28,29], Skyrme energy density functional [30,31], Hartree-Fock with random phase approximation [32], relativistic mean field with random phase approximation predicated on effective Lagrangians with density-dependent meson-nucleon vertex functions [33], among other many-body approaches, have been employed to study the symmetry energy of finite nuclei at a local density approximation. In parallel to these, the well-known Brückner energy density functional [34,35] within the coherent density fluctuation model as those in Refs. [8,11,36,37] is successfully applied for the study of surface properties of nuclei. It is well known that the classical Brückner energy density functional fails to satisfy the Coester-Band problem [38,39], i.e., inability to accurately reproduce the empirical saturation density $\rho \approx 0.15$ fm^{-3} and binding energy per nucleon in the limit $E/A \approx -16$ MeV [40]. Later on, a few alternative attempts which considered the incorporation of various realistic

*jeetamritboudh@gmail.com
†majekjoe1@gmail.com
‡ankit.k@iopb.res.in
§bunuphy@um.edu.my
‖patra@iopb.res.in

nucleon-nucleon potentials [38,41] into the Brückner energy density functional are found either to overestimate the nuclear matter density or underestimate the binding energy. In other words, the saturation properties must satisfy the nuclear equation of state while extrapolating to higher density and isospin asymmetry.

Recently, the surface properties of nuclei can be estimated by using the nonrelativistic and relativistic inputs within the coherent density fluctuation model [8,11,12,36,37]. From these analyses, one can find the notable peaks and/or kinks that have been observed for traditional magic neutron and/or proton, for example, $N = 20, 28$ for Ca and $N = 82$ for Sn along with a few predictions for drip line and superheavy island [8,10–12,36,37]. On the other hand, these studies are unable to reproduce peaks and kinks for Pb ($N = 126$), which may be associated with the saturation properties. In this context, it necessitates a well-grounded approach that can both tackle the Coester-Band problem [38,39] as well as the suprasaturation object including neutron star. In our previous work, a newly fitted relativistic density functional has been introduced [42] and tested for a few double magic nuclei. Hence, it is our main objective to test the newly relativistic energy density functional for the isotopic chain of Pb nuclei. In the present analysis, the symmetry energy and its volume and surface components are calculated by using the relativistic energy density functional, which stems from the effective-field theory motivated relativistic mean-field model [43,44] for the well-known NL3 and recently developed G3 parameter sets.

The paper is organized as follows: Section II describes briefly the relativistic mean-field approach along with the coherent density fluctuation model. The results obtained from the calculations are discussed in Sec. III and a concise summary and conclusions are presented in Sec. IV.

II. RELATIVISTIC ENERGY DENSITY FUNCTIONAL

The effective field theory motivated relativistic mean-field approach is constructed by taking the interactions of isoscalar (scalar σ, vector ω) and isovector (scalar δ, vector ρ) mesons with nucleons and among themselves. The crossed coupling of mesons up to fourth order is also included. The relativistic mean field is known to be highly successful in reproducing the ground-state properties of not only β-stable nuclei but also provides a plausible prediction of the properties of drip lines and superheavy nuclei [43,44]. Lately, this formalism has gained a wide range of application in nuclear astrophysics. In particular, it describes the structure of neutron star and gives an accurate prediction of the tidal deformability [45]. Exhaustive details on the relativistic mean-field Lagrangian and parametrization can be found in Refs. [42–44,46,47]. The energy density $\mathcal{E}_{\text{nucl.}}$ [42–44] is obtained by assuming that an uniform field is created by the exchange of mesons, where the oscillation of nucleons is considered as a simple harmonic motion. From the relativistic mean field energy density, the equation of motions for the mesons and the nucleons are obtained from the Euler-Lagrange equation. A set of coupled differential equations are obtained and solved self-consistent manner [44]. The scalar and vector densities are given as

$$\rho_s(r) = \sum_{\alpha} \varphi_{\alpha}^{\dagger}(r)\beta\varphi_{\alpha}, \tag{1}$$

$$\rho_v(r) = \sum_{\alpha} \varphi_{\alpha}^{\dagger}(r)\tau_3\varphi_{\alpha}, \tag{2}$$

and deduced from the converged solutions within spherical harmonics. $\rho_v(r)$ in Eq. (2) is used within coherent density fluctuation model to obtain the weight function $|F(x)|^2$ with which the symmetry energy S^A is obtained.

The energy density of infinite and isotropic nuclear matter are deduced from the energy-momentum tensor:

$$T_{\mu\nu} = \sum_i \partial_\nu \phi_i \frac{\partial \mathcal{L}}{\partial(\partial^\mu \phi_i)} - g_{\mu\nu}\mathcal{L}. \tag{3}$$

The zeroth component of the energy-momentum tensor T_{00} gives the energy density of the system as a function of scalar and vector density ρ_s and ρ_v respectively [42]:

$$\begin{aligned}\mathcal{E}(k)_{\text{nucl.}} = {} & \frac{2}{(2\pi)^3}\int d^3k E_i^*(k) + \frac{m_s^2\Phi^2}{g_s^2}\left(\frac{1}{2} + \frac{\kappa_3}{3!}\frac{\Phi}{M}\right. \\ & \left. + \frac{\kappa_4}{4!}\frac{\Phi^2}{M^2}\right) + \rho_b W - \frac{1}{4!}\frac{\zeta_0 W^4}{g_\omega^2} - \frac{1}{2}m_\omega^2\frac{W^2}{g_\omega^2} \\ & \times \left(1 + \eta_1\frac{\Phi}{M} + \frac{\eta_2}{2}\frac{\Phi^2}{M^2}\right) + \frac{1}{2}\rho_3 R - \frac{1}{2}\left(1 + \frac{\eta_\rho\Phi}{M}\right) \\ & \times \frac{m_\rho^2}{g_\rho^2}R^2 - \Lambda_\omega(R^2 \times W^2) + \frac{1}{2}\frac{m_\delta^2}{g_\delta^2}D^2. \end{aligned} \tag{4}$$

A. E-RMF fitting procedure

The conversion of the nuclear matter quantities [Eq. (4)] from momentum space to the coordinate space is the major distinction of the calculation. In other words, the nuclear matter quantities are reconstructed at local density. It is assumed that the nuclear matter is made up of tiny spherical pieces described by a local density function termed as *flucton* and defined as $\rho_0(x) = 3A/4\pi x^3$. As such, the fitted binding energy function of relativistic mean field is expressed as [42]

$$\mathcal{E}(x) = C_k\rho_0^{2/3}(x) + \sum_{i=3}^{14}(b_i + a_i\alpha^2)\rho_0^{i/3}(x). \tag{5}$$

The first term represents the kinetic energy, whose coefficient C_k is given as $C_k = 37.53[(1+\alpha)^{5/3} + (1-\alpha)^{5/3}]$ following the Thomas-Fermi approach. The asymmetry parameter α is defined as $\alpha = \frac{\rho_n - \rho_p}{\rho_n + \rho_p}$, with ρ_n and ρ_p being the neutron and proton density distributions, respectively. A number of terms are involved in the polynomial fitting [Eq. (5)], which is used to obtain the exact nature of the binding per particle E/A in position space. The mean deviation is calculated using the formula $\delta = [\sum_{j=1}^{n}(E/A)_{j,\text{Fitted}} - (E/A)_{j,\text{RMF}}]/n$. The term $(E/A)_{j,\text{Fitted}}$ represents the binding energy deduced from Eq. (5), $(E/A)_{j,\text{RMF}}$ is the binding energy per nucleon from the relativistic mean field (RMF) functional, and n is the number of data points. From the analysis [42], it is found that 12 terms are considered to obtain the best fit and the

coefficients extrapolated from the polynomial fitting are presented in Table I of Ref. [42].

The nuclear matter symmetry energy $S^{\rm NM}$ is obtained from the following standard relations [44,48],

$$S^{\rm NM} = \frac{1}{2}\frac{\partial^2(\mathcal{E}/\rho)}{\partial\alpha^2}\bigg|_{\alpha=0}, \tag{6}$$

which is given as follow using Eqs. (2) and (3):

$$S^{\rm NM} = 41.7\,\rho_0^{2/3}(x) + \sum_{i=3}^{14} a_i\,\rho_0^{i/3}(x). \tag{7}$$

The density of closed and semiclosed shell spherical Pb nucleus is calculated using relativistic mean field formalism and used as input in the coherent density fluctuation model to calculate the weight function, which is the major quantity that bridges nuclear matter parameters in x space and finite nuclei in r space using local density approximation. The r and x space are matched together, by the superposition of the total density of the nucleus and an infinite number of fluctons, using the coherent density fluctuation model approach.

B. Brückner's prescription

The expression for the energy density of infinite and isotropic nuclear matter are obtained from the Brückner functional defined as [34,35]

$$\mathcal{E}(\rho)_{\rm nucl.} = AV_0(x) + V_C - V_{Cx}, \tag{8}$$

where

$$\begin{aligned} V_0(x) = {} & 37.53[(1+\alpha)^{5/3} + (1-\alpha)^{5/3}]\rho_0(x)^{2/3} \\ & + b_1\rho_0(x) + b_2\rho_0(x)^{4/3} + b_3\rho_0(x)^{5/3} \\ & + \alpha^2[b_4\rho_0(x) + b_5\rho_0(x)^{4/3} + b_6\rho_0(x)^{5/3}]. \end{aligned} \tag{9}$$

Here, $b_1 = -741.28$, $b_2 = 1179.89$, $b_3 = -467.54$, $b_4 = 148.26$, $b_5 = 372.84$, $b_6 = -769.57$ and the total density $\rho = \rho_n + \rho_p$ is the sum of the neutron and proton density distributions [9]. In each fluctons, there are protons having Coulomb energy $V_C = \frac{3}{5}\frac{Z^2e^2}{x}$ and Coulomb exchange energy $V_{Cx} = 0.7386Ze^2(3Z/4\pi x^3)^{1/3}$. The important part of the present calculation is to convert the nuclear matter quantities in Eq. (8) from momentum (ρ) to coordinate (r) space in the local density approximation. The nuclear matter symmetry energy parameter $S^{\rm NM}$ is obtained from the well-defined relation [36,44,48]:

$$\begin{aligned} S^{\rm NM} &= \frac{1}{2}\frac{\partial^2(\mathcal{E}/\rho)}{\partial\alpha^2}\bigg|_{\alpha=0} \\ &= 41.7\rho_0(x)^{2/3} + b_4\rho_0(x) + b_5\rho_0(x)^{4/3} + b_6\rho_0(x)^{5/3} \end{aligned} \tag{10}$$

at local density. The weight function $|F(x)|^2$ for a given density ρ (r) is defined as

$$|F(x)|^2 = -\left(\frac{1}{\rho_0(x)}\frac{d\rho(r)}{dr}\right)_{r=x}, \tag{11}$$

with $\int_0^\infty dx|F(x)|^2 = 1$. More comprehensive analytical derivations are found in Refs. [8,36,37,49,50]. Here the relativistic mean-field densities obtained from G3 and NL3 parameter sets are used as local density to calculate the weight function as defined in Eq. (11). The densities near the surface region monotonically decrease for finite nuclei, which produces a peak in the weight function for this region. It is to be noted that the peak of the weight function appears in the tail part of the density distribution. Further discussion is given below in the result section with Fig. 1. The coherent density fluctuation model provides an easy transition from the properties of nuclear matter to those of finite nuclei. The finite nucleus symmetry energy S^A with mass number A is calculated by weighting the corresponding quantity for infinite nuclear matter within the coherent density fluctuation model, as given below [36,37,51]:

$$S^A = \int_0^\infty dx\,|F(x)|^2\,S^{NM}(\rho(x)). \tag{12}$$

The symmetry energy S^A in Eq. (12) is the surface-weighted average of the corresponding nuclear matter quantity in the local density approximation limit for finite nuclei. To estimate the symmetry energy, the densities are obtained self-consistently from relativistic mean field and folded with the nuclear matter parameters using the coherent density fluctuation model.

The surface S_S^A and volume S_V^A components of symmetry energy are analyzed separately in the framework of Danielewicz's liquid drop model [52–54]. The symmetry energy S^A is connected with the surface and volume components as [55]

$$S^A = \frac{S_V^A}{1 + \frac{S_S^A}{S_V^A}A^{-1/3}} = \frac{S_V^A}{1 + A^{-1/3}/\kappa}. \tag{13}$$

From Eq. (13), the individual components of S_V^A and S_S^A can be written as

$$S_V^A = S^A\left(1 + \frac{1}{\kappa A^{1/3}}\right) \tag{14}$$

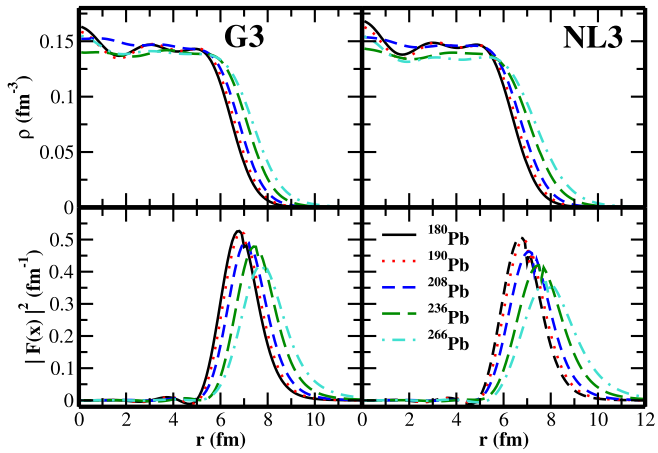

FIG. 1. The relativistic mean field densities and weight functions for ^{180,190,208,236,266}Pb with NL3 and G3 parameter sets. The densities of ^{180,190,208,236,266}Pb nuclei are shown in upper panel with solid, dotted, short dashed, long dashed, and dot-dashed lines, respectively. The same are shown for the weight function $|F(x)|^2$ but in the lower panel.

and

$$S_S^A = \frac{S^A}{\kappa}\left(1 + \frac{1}{\kappa A^{1/3}}\right). \tag{15}$$

Here, $\kappa \equiv \frac{S_V^A}{S_S^A}$ is the ratio of the volume and surface symmetry energy. The symmetry energy, its volume, and surface components are calculated within the coherent density fluctuation model formalism [8,9,52–57]. Recently, an alternative approach has been introduced by Gaidarov *et al.* to obtain the volume and surface symmetry energy components by taking the nonrelativistic densities in the weight function [57].

III. RESULTS AND DISCUSSIONS

A. Density and weight function $|F(x)|^2$

Figure 1 represents the densities of three different regions of Pb isotopic series. We have considered the densities of ^{180}Pb, ^{190}Pb, ^{208}Pb, ^{236}Pb, and ^{266}Pb for the β stable and drip-line regions as representative cases ranging from the neutron-deficient, β-stable, and neutron-rich regions, which analyse the relative changes of the density with respect to neutron-proton isospin asymmetry. From the relativistic mean-field density, we acquire the weight function $|F(x)|^2$ of the nucleus. Here, $|F(x)|^2$ is one of the crucial factors to determine the surface properties of the nucleus. This value is significant with a radial distribution of ≈5–10 fm for ^{180,190,208}Pb and ≈5–12 fm for ^{236,266}Pb, showing the surface properties of the nuclei (see lower panel of Fig. 1), because this region of the nucleus lies in the tail part of the density distribution of nucleons as shown in the upper panel of Fig. 1.

B. Symmetry energy

The peak in the surface properties such as nuclear symmetry energy and its component are used as indicators of shell and subshell closure [8,11,12,36,37]. The possible reasons for the disappearance of the peak at neutron number $N = 126$ for Pb nuclei have been discussed. It is reported that the peak shifted a few units ($N = 120$) than $N = 126$ when the Brückner energy density functional is used in the evaluation of symmetry energy within the coherent density fluctuation model formalism. The use of the self-consistent relativistic mean field density does not improve the situation much. To see the effect on the functional chosen, here the recently developed relativistic energy density functional [42], which systematically incorporates the Coester-Band problem [38,39] via the relativistic mean-field Lagrangian density, is compared to the conventional Brückner functional.

Figure 2 displays the profile of the symmetry energy S^A as a function of neutron numbers ranging from $N = 98$ to $N = 184$ for Pb isotopes. Here, only the even-even nuclei are considered to preserve the time-reversal symmetry and also avoid the odd-even staggering. A comparison is made between the symmetry energy obtained from Brückner (green open diamonds) and relativistic energy density functionals (black open circles) to assert their respective suitability in the Pb isotopic chain. Although the trends seem to be somewhat similar, both predictions fall between different ranges

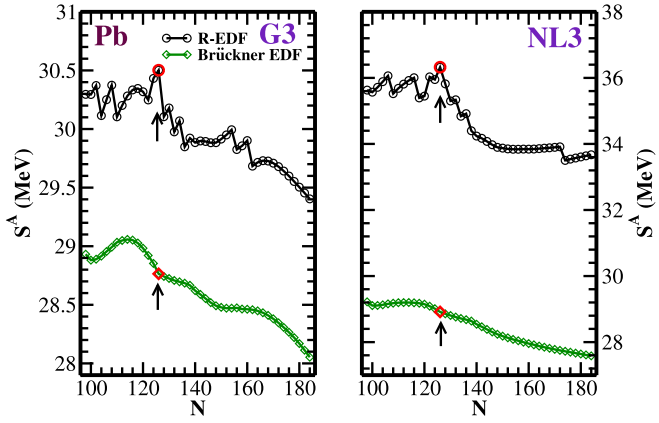

FIG. 2. The nuclear symmetry energies are shown for the relativistic energy density and Brückner energy density functionals for the Pb isotopes with G3 (open circle) and NL3 (open diamond) parameter sets. The arrow represents the value of S^A at $N = 126$.

of values. In other words, Brückener's predicted values are bounded between 28.0 and 29.2 MeV while those from relativistic mean field with G3 force parameter are found between 29.4 and 30.6 MeV over the isotopic chain. Similarly, for NL3 set, the Brückner's prediction is in the range 27.5–29.2 MeV and the relativistic energy density functional result is in between 33.6 and 35.7 MeV for the considered Pb chain. The symmetry energy at saturation for nuclear matter with G3 and NL3 forces are 31.8 and 37.4 MeV, respectively [43,44]. At $N = 126$, the symmetry energy of the relativistic energy density functional differs by 1.73 MeV for G3 from its Brückner prediction, whereas this difference for NL3 is 7.40 MeV. This implies the relativistic mean-field approach gives larger symmetry energy than the Brückner approach. Further, we noticed few maxima and minima in the relativistic mean-field prediction of symmetry energy both in G3 and NL3 models, indicating the structure effect of the isotopic chain. However, these variations in S^A are very small and cannot be considered as the shell-subshell closure. In the case of NL3, few other maxima appears in the symmetry energy curve. Although these peaks almost comparable with $N = 126$, we do not consider those as shell-subshell closures because of the small fluctuation in the values of S^A. Mostly we respect the trend of the curve while locating the shell-subshell closure as shown in Fig. 2. Furthermore, from Brückner's prescription, no significant peak is found at the $N = 126$ shell closure, corresponding to ^{208}Pb as also reported in earlier studies [8,11,12,36,37] and the references therein. This peak shifted to $N = 120$ which is not a closed shell for Pb nucleus. In contrast, interestingly, the relativistic energy density functional shows a notable peak at the neutron shell closure $N = 126$ in G3 and NL3 parameter sets. More careful inspection shows that the trajectories of the symmetry energy exhibits an anomalous trend in both cases, which is very common in the mean-field calculation due to the structure effect of the nucleus. Although the predictions for both parameter sets have different magnitude, it is obvious that they are characterized with the same trends for the shell-subshell closure. This indicates that the relativistic energy density functional predictions for shell-subshell closure

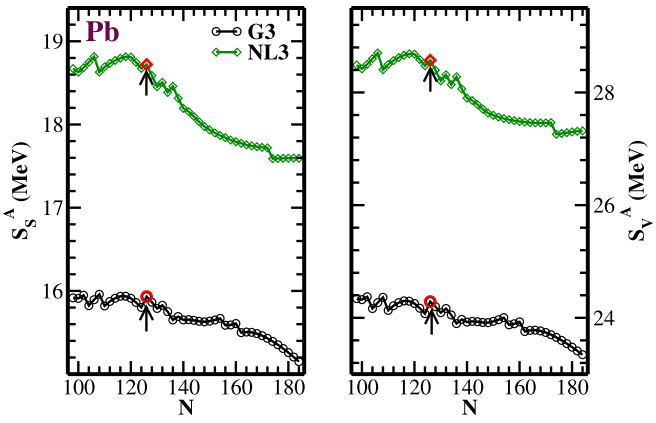

FIG. 3. The surface (S_S^A) and volume (S_V^A) symmetry energies are estimated using Danielewicz's liquid drop prescription for the Pb isotopes with G3 (open circle) and NL3 (open diamond) parameter sets. The arrow represents the symmetry energy at neutron number $N = 126$.

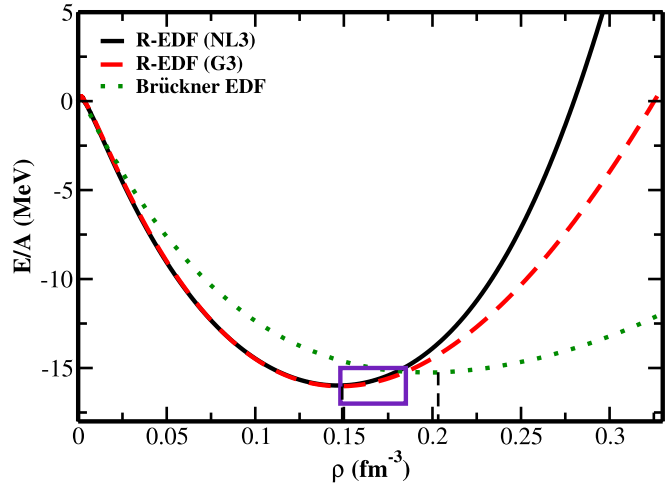

FIG. 4. Binding energy per particle (E/A) as a function of nuclear matter density (ρ) for NL3 (black solid), G3 (red dashed), and Brüeckner energy density functionals (green dotted). The rectangular box indicates the Coester band with empirical density and binding energy per nucleon [38,39].

within surface properties such as symmetry energy and its components are merely sensitive to the choice parameter set used.

C. Volume and surface components of symmetry energy

Figure 3 displays the variation of S_S^A and S_V^A over the Pb-isotopic chain as a function of the neutron number N. There exists a strong correlation between the parameters S_S^A and S_V^A. Although a similar trend is observed in their profiles, it is clear that their respective magnitudes vary with their neutron numbers and they are bound between different energy ranges. In particular, from their respective values, the volume component contributes more to the symmetry energy. In both cases, a notable peak or kink is found at the neutron shell closure $N = 126$. Again, the NL3 predictions seem to be characterized with lesser undulations and/or fluctuations as compared to the G3 parameter set. One of the striking observations in the relativistic energy density functional framework is that parametrization plays a key role in its calculations. More elaborate details on the surface and volume components of the symmetry energy as well as their parametrizations and respective contributions can be found in Refs. [58,59].

D. Coester-band problem

Having obtained a peak at $N = 126$ using the relativistic energy density functional with the G3 and NL3 parameter sets, it is yet necessary to validate the appropriateness of this functional in the wake of the Coester-band problem. Figure 4 shows the variation of the nuclear matter binding energy per nucleon E/A as function of the baryonic density for symmetric nuclear matter with the Brückner (green dotted line) and relativistic mean-field (G3 and NL3 with red dashed and black solid lines respectively) functionals. Relatively, one can vividly notice that while E/A shifts toward the lower density region, the deepest minimum in the Brückner's prescription turns out to underestimate E/A as -14.9 MeV and overestimate the saturation density ρ to be ≈ 0.2 fm^{-3}. In the case of a relativistic energy density functional, the deepest minimum passes through the band at $E/A = -16$ MeV and $\rho = 0.15$ fm^{-3} rather than the empirical one as shown in the rectangular box [38,39]. This resolves the issue of the Coester-band problem [38,39], which is directly connected with the energy density, and the isospin-dependant quantities such as symmetry energy and its component and/or coefficient. Hence, the dilute picture of peak at the magic number in the case of Brückener's functional can be correlated with the Coester-band problem. In other words, the successful achievement of the Coester-band problem within relativistic energy density functional is reflected in the calculation of symmetry energy and its component and reproduce the peak of Pb isotopes at $N = 126$, contrary to Brückner's functional at $N = 120$. This shifting of the peak from $N = 126$ to $N = 120$ may be correlated with the shifting of the energy minimum to the Fermi momentum value $k_f \approx 2.0$ fm^{-3}.

IV. SUMMARY AND CONCLUSIONS

The surface properties of Pb isotopes are evaluated using the newly fitted expression of Ankit *et al.* derived from relativistic mean-field formalism to resolve the Coester-band problem encountered in the conventional Brückner energy density functional. The relativistic mean-field densities with the NL3 and G3 parameter sets are used as inputs to obtain the weight function within the coherent density fluctuation model. The relativistic energy density functional manifests a remarkable success in accurately reproducing the empirical saturation density ρ as well as the binding energy per nucleon E/A. Hence, it is established that this approach has an edge over the Brückner's prescription.

Besides, the relativistic energy density functional is used to establish the existence of peak in the symmetry energy of finite nuclei over the Pb isotopic chain at $N = 126$ corresponding to the double magic ^{208}Pb nucleus, which has been

hitherto elusive within the conventional Brückner's prescription. Although the trend in the Pb-isotopic chain is not smooth enough (especially with the G3 parameter set), a careful inspection reveals that the relativistic energy density functional is susceptible to the choice of parameter set and may be a manifestation of the structure effects of the nucleus. In other words, a smoother behavior is observed using the NL3 parameter set. This infers that the result could be improved by choosing an appropriate parameter set and taking into account the proper structure effects.

ACKNOWLEDGMENTS

One of the authors (J.A.P.) is thankful to the Institute of Physics, Bhubaneswar, for providing computer facilities during the work. SERB partly supports this work, Department of Science and Technology, Govt. of India, Project No. CRG/2019/002691. M.B. acknowledges the support from FOSTECT Project No. FOSTECT.2019B.04, FAPESP Project No. 2017/05660-0, and the CNPq, Brazil. J.T.M. acknowledges support from FRGS Grant No. FRGS/1/2019/STG02/UniMAP/02/2.

[1] T. Nikšić, D. Vretenar, and P. Ring, Phys. Rev. C **78**, 034318 (2008).
[2] S. K. Singh, S. K. Biswal, M. Bhuyan, and S. K. Patra, J. Phys. G: Nucl. Part. Phys. **41**, 055201 (2014).
[3] E. van Dalen and H. Muther, Int. J. Mod. Phys. E **19**, 2077 (2010).
[4] L. W. Chen, C. M. Ko, B. A. Li, and G. C. Yong, Int. J. Mod. Phys. E **17**, 1825 (2008).
[5] B.-A. Li, P. G. Krastev, D.-H. Wen, and N.-B. Zhang, Eur. Phys. J. A **55**, 117 (2019).
[6] N. B. Zhang and B. A. Li, J. Phys. G **46**, 014002 (2019).
[7] A. N. Antonov, M. K. Gaidarov, P. Sarriguren, and E. Moya de Guerra, Phys. Rev. C **94**, 014319 (2016).
[8] M. Bhuyan, B. V. Carlson, S. K. Patra, and S.-G. Zhou, Phys. Rev. C **97**, 024322 (2018).
[9] M. Kaur, A. Quddus, A. Kumar, M. Bhuyan, and S. K. Patra, Nucl. Phys. A **1000**, 121871 (2020).
[10] M. Kaur, A. Quddus, A. Kumar, M. Bhuyan, and S. K. Patra, J. Phys. G: Nucl. Part. Phys. **47**, 105102 (2020).
[11] A. Quddus, M. Bhuyan, and S. K. Patra, J. Phys. G: Nucl. Part. Phys. **47**, 045105 (2020).
[12] J. A. Pattnaik, M. Bhuyan, R. N. Panda, and S. K. Patra, Phys. Scr. **96**, 125319 (2021).
[13] M. Thoennessen, Nucl. Phys. A **834**, 688c (2010).
[14] H. Sakurai, Nucl. Phys. A **805**, 526c (2008).
[15] H. Geissel, P. Armbruster, K. H. Behr, A. Brünle, K. Burkard, M. Chen, H. Folger, B. Franczak, H. Keller, O. Klepper *et al.*, Nucl. Instrum. Methods Phys. Res. Sect. B **70**, 286 (1992).
[16] A. M. Rodin *et al.*, Nucl. Instrum. Methods Phys. Res. Sect. B **204**, 114 (2003).
[17] Z. Sun, W. L. Zhan, Z. Y. Guo, G. Xiao, and J. X. Li, Nucl. Instrum. Methods Phys. Res. Sect. A **503**, 496 (2003).
[18] A. C. Mueller and R. Anne, Nucl. Instrum. Methods Phys. Res. Sect. B **56-57**, 559 (1991).
[19] B. A. Li, L. W. Chen, and C. M. Ko, Phys. Rep. **464**, 113 (2008).
[20] T. Motobayashi, EPJ Web Conf. **66**, 01013 (2014).
[21] P. Decrock, T. Delbar, P. Duhamel, W. Galster, M. Huyse, P. Leleux, I. Licot, E. Liénard, P. Lipnik, M. Loiselet *et al.*, Phys. Rev. Lett. **67**, 808 (1991).
[22] R. Boussaid, G. Ban, J. F. Cam, and C. Vandamme, J. Instrument. **9**, P07009 (2014).
[23] S. Franchoo, JPS Conf. Proc. **6**, 020041 (2015).
[24] S. Essabaa *et al.*, Nucl. Instrum. Methods Phys. Res. Sect. B **317**, 218 (2013).
[25] M. P. Reiter *et al.*, Nucl. Instrum. Methods Phys. Res. Sect. B **463**, 431 (2020).
[26] M. A. Fraser, Y. Kadi, A. P. Bernardes, Y. Blumenfeld, E. Bravin, S. Calatroni, R. Catherall, B. Goddard, D. Parchet, E. Siesling *et al.*, arXiv:1707.05129v1.
[27] N. Van Giai, B. V. Carlson, Z. Ma, and H. Wolter, J. Phys. G **37**, 064043 (2010).
[28] W. D. Myers and W. J. Swiatecki, Nucl. Phys. **81**, 1 (1966).
[29] K. Pomorski and J. Dudek, Phys. Rev. C **67**, 044316 (2003).
[30] L. W. Chen, C. M. Ko, B.-A. Li, and J. Xu, Phys. Rev. C **82**, 024321 (2010).
[31] M. Dutra, O. Lourenco, J. S. Sá Martins, A. Delfino, J. R. Stone, and P. D. Stevenson, Phys. Rev. C **85**, 035201 (2012)
[32] A. Carbone, G. Colò, A. Bracco, L.-G. Cao, P. F. Bortignon, F. Camera, and O. Wieland, Phys. Rev. C **81**, 041301(R) (2010).
[33] D. Vretenar, T. Nikšić, and P. Ring, Phys. Rev. C **68**, 024310 (2003).
[34] K. A. Brückner, J. R. Buchler, S. Jorna, and R. J. Lombard, Phys. Rev. **171**, 1188 (1968).
[35] K. A. Brückner, J. R. Buchler, R. C. Clark, and R. J. Lombard, Phys. Rev. **181**, 1543 (1969).
[36] M. K. Gaidarov, A. N. Antonov, P. Sarriguren, and E. Moya de Guerra, Phys. Rev. C **84**, 034316 (2011).
[37] M. K. Gaidarov, A. N. Antonov, P. Sarriguren, and E. M. de Guerra, Phys. Rev. C **85**, 064319 (2012).
[38] F. Coester, S. Cohen, B. Day, and C. M. Vincent, Phys. Rev. C **1**, 769 (1970).
[39] R. Brockmann and R. Machleidt, Phys. Rev. C **42**, 1965 (1990).
[40] W. D. Myers and W. J. Swiatecki, Nucl. Phys. A **601**, 141 (1996).
[41] B. D. Day, Phys. Rev. Lett. **47**, 226 (1981).
[42] A. Kumar, H. C. Das, M. Kaur, M. Bhuyan, and S. K. Patra, Phys. Rev. C **103**, 024305 (2021).
[43] B. Kumar, S. Singh, B. Agrawal, and S. K. Patra, Nucl. Phys. A **966**, 197 (2017).
[44] B. Kumar, S. K. Patra, and B. K. Agrawal, Phys. Rev. C **97**, 045806 (2018).
[45] T. Malik, N. Alam, M. Fortin, C. Providência, B. K. Agrawal, T. K. Jha, B. Kumar, and S. K. Patra, Phys. Rev. C **98**, 035804 (2018).
[46] R. Furnstahl, B. D. Serot, and H.-B. Tang, Nucl. Phys. A **598**, 539 (1996).
[47] R. Furnstahl, B. D. Serot, and H.-B. Tang, Nucl. Phys. A **615**, 441 (1997).
[48] W.-C. Chen and J. Piekarewicz, Phys. Rev. C **90**, 044305 (2014).
[49] A. N. Antonov, V. A. Nikolaev, and I. Z. Petkov, Z. Phys. A: At. Nucl. **297**, 257 (1980).

[50] A. N. Antonov, V. A. Nikolaev, and I. Z. Petkov, Nuovo Cimento A **86**, 23 (1985).
[51] A. N. Antonov, D. N. Kadrev, M. K. Gaidarov, P. Sarriguren, and E. M. de Guerra, Phys. Rev. C **95**, 024314 (2017).
[52] P. Danielewicz, Nucl. Phys. A **727**, 233 (2003).
[53] P. Danielewicz, arXiv:nucl-th/0411115.
[54] P. Danielewicz, in *Opportunities with Exotic Beams* (World Scientific, Singapore, 2007), pp. 142–151.
[55] A. Steiner, M. Prakash, J. Lattimer, and P. Ellis, Phys. Rep. **411**, 325 (2005).
[56] I. C. Danchev, A. N. Antonov, D. N. Kadrev, M. K. Gaidarov, P. Sarriguren, and E. Moya de Guerra, Phys. Rev. C **101**, 064315 (2020).
[57] M. K. Gaidarov, E. Moya de Guerra, A. N. Antonov, I. C. Danchev, P. Sarriguren, and D. N. Kadrev, Phys. Rev. C **104**, 044312 (2021).
[58] B. K. Agrawal, J. N. De, and S. K. Samaddar, Phys. Rev. Lett. **109**, 262501 (2012).
[59] W. Satula, R. A. Wyss, and M. Rafalski, Phys. Rev. C **74**, 011301(R) (2006).